Phase transitions and mechanical behavior of Ti-3wt.%Nb alloy after high pressure torsion and low-temperature annealing

A. Korneva [a,*], B. Straumal [b], A. Kilmametov [b], S. Kopacz [c], M. Szczerba [a], Ł. Gondek [d], G. Cios [e], L. Lityńska-Dobrzyńska [a], R. Chulist [a]

[a] Institute of Metallurgy and Materials Science, Polish Academy of Sciences, 30-059, Krakow, Poland
[b] Karlsruhe Institute of Technology (KIT), Institute of Nanotechnology, 76344 Eggenstein-Leopoldshafen, Germany
[c] AGH University of Science and Technology, Faculty of Non-Ferrous Metals, 30-059, Kraków, Poland
[d] AGH University of Science and Technology, Faculty of Physics and Applied Computer Science, 30-059, Kraków, Poland
[e] AGH University of Science and Technology, Academic Centre of Materials and Nanotechnology, 30-059, Kraków, Poland

ARTICLE INFO

Keywords:
Ti alloys
Phase transitions
High pressure torsion
In situ XRD
Mechanical behavior

ABSTRACT

The influence of microstructure and phase transitions on tensile strength, plasticity and microhardness of a Ti-3wt.%Nb alloy subjected to high pressure torsion (HPT) followed by annealing is studied in this work. The initial state of the alloy was the α-solid solution with a small amount of the β-precipitates. The characterization of microstructure and phase transitions has been performed using scanning and transmission electron microscopy as well as X-ray diffraction. During HPT, the grain refinement took place and the α-phase partially transformed into ω-phase. The tensile test of the HPT-deformed sample showed an almost two-fold increase of ultimate strength in comparison with the initial state, as well as lower plasticity. During the short-term annealing of the deformed state up to 250 °C, the grain size slightly increased, the density of the crystal structure defects decreased and ω-phase transformed back to the α-phase. Such microstructural changes led to an important growth of plasticity and a slight decrease in ultimate strength of the HPT-deformed alloy.

1. Introduction

The titanium alloys doped by Nb are very promising for application as metallic biomaterials (in particular, as orthopaedic implants) for a number of reasons. Among them are their low Young's modulus, which is comparable with Young's modulus of human bone, good biocompatibility of Ti and Nb in their bulk state, and excellent corrosion resistance [1-4]. However, the Ti–Nb-based alloys are now only seldom used in orthopaedics due to lower strength in comparison with widely applied biocompatible Ti-alloys like Ti–6Al–7Nb, Ti–5Al-2.5Fe or Ti–6Al–4V ones which possess restricted biocompatibility and relatively high Young's modulus [2,5].

Various methods of severe plastic deformation (SPD) can be successfully applied for improving the mechanical properties of metallic materials [6-8]. For example, the high-temperature deformation of Grade-2 purity titanium by equal-channel angular pressing (ECAP) increases its yield strength from 330 to 652 MPa due to strong grain refinement up to the nanoscale and an increase in dislocations density [9]. The study of high-pressure torsion (HPT) effect on the microstructure and mechanical properties of commercially pure titanium (Grade 4) showed that the ultimate tensile strength after HPT processing reaches 1600 MPa as a result of significant grain refinement of the microstructure [10]. On the other hand, the subsequent annealing of the HPT-treated samples strongly influences their ductility [10]. Improvement in the strength characteristics of Ti-based alloys by SPD can also be found in many works, where these changes can be associated with the β → α″ [11-14] or β → α phase transformation [15]. Therefore, SPD is quite effective for stimulating allotropic transformations.

Many properties of Ti–Nb alloys are connected with the β-α allotropic phase transition in Ti at 882 °C. The high temperature β-Ti phase has a body-centred cubic lattice, the low temperature α-Ti phase has a hexagonal closely packed lattice. Depending on the chemical composition and heat treatment, Ti–Nb alloys could also contain metastable α′ or α″martensite and as well as hexagonal ω-phase. The α′-phase has hexagonal closely packed lattice and the α″martensite has orthorhombic structure and they may form by quenching the β-phase. The β→a″transformation takes place in the Ti–Nb binary alloys instead of the β→a' one above 11–13 wt% Nb [11]. The ω-phase can be obtained as a

* Corresponding author.
E-mail address: a.korniewa@imim.pl (A. Korneva).

result of slow quenching of β phase ($\omega_{athermal}$), during isothermal aging of β phase ($\omega_{isothermal}$) or under high-pressure of β phase and can retain after pressure release [4,16,17]. It was found that α-Ti as well transforms into ω-phase under hydrostatic pressure 2–12 GPa [18-20]. The SPD induced α → ω and β → ω transformations are martensitic (diffusionless). They are promoted both by shear strain under SPD and alloying of Ti with so-called β-stabilisers (like Fe, Co, Nb, Ni, Mo). The HPT-induced α → ω [18,21-23], β → ω [24], α' → ω [25] and α″→ ω [26] transformations and the thermal stability of the SPD-induced ω-phase [18,27-29] in Ti-based alloys have been studied recently. However, only a very small number of papers are devoted to the influence of the ω-phase on the mechanical behaviour of the SPD-treated Ti-based alloys. Moreover, among the mechanical properties, the values of hardness and Young's modulus are usually measured [22,23,26,29-31], while there are practically no data on the tensile strength. This is probably due to the fact that the ω-phase leads to a severe loss of ductility and an increase in the hardness of the material.

It follows from a review of the literature that the use of short-term, low-temperature annealing before tensile testing [32,33] or tension at elevated temperatures [22,34] can lead to an improvement in the plasticity of HPT-deformed alloys. For example, the short-term annealing of HPT-treated titanium at 200–300 °C increased both ductility and strength [32,33]. The annealing decreased significantly the lattice distortions without measurable grain growth. The authors of the works [32, 33] stated that the observed changes in the mechanical behaviour closely correlated with the changes of grain boundary (GB) structure. These changes are due to the rearrangement of defects (like vacancies, interstitials or dislocations), which moved during SPD from grain interior to the near-GB regions. Nevertheless, the metastable ω-phase in the pure Ti remains in the HPT deformed samples only up to 180 °C [18]. Therefore, the observed changes of the mechanical properties under annealing could also be due to the ω → α back transformation. The important increase in ductility together with slight decrease of ultimate strength was also observed in the Zr-2.5 wt%Nb alloy after HPT and low-temperature annealing [34], where these changes in the properties were correlated with a partial reverse ω → α phase transformation. Therefore, the application of the HPT process and additional annealing is very promising approach for producing advanced metallic biomaterials with high level of mechanical properties.

The goal of this study is to analyse the effect of microstructure and phase transformations (α → ω, ω → α) on the mechanical properties (tensile strength, plasticity and microhardness) of a Ti-3wt.%Nb alloy subjected to HPT at room temperature followed by low-temperature annealing. This work is a continuation of earlier studies [31], where the main goal was to investigate the niobium influence on the peculiarities of the HPT-driven α→ω phase transformation in the Ti-3wt.%Nb alloy previously annealed at different temperatures.

2. Material and methods

2.1. Preparation of the research material

The Ti–3wt.%Nb alloy was prepared from pure components (99.98% Ti and 99.99% Nb) by the induction melting in an atmosphere of pure argon in form of 10 mm diameter cylindrical ingots. They were then cut by spark erosion into the 0.7 mm thin slices. The slices were individually sealed in quartz ampoules with remaining pressure of 10^{-4} Pa. The quartz ampoules were annealed at 600 °C for 888 h. This temperature is in the stability area of α-phase. The long annealing time was selected in order ensure the equilibrium niobium content in the α-solid solution. After annealing the samples were water quenched (together with ampoules). The resulted samples were HPT-treated at the pressure of 7 GPa, 5 anvil rotations with a speed of 1 rpm. The Bridgman anvil type custom built computer-controlled device was used produced by W. Klement GmbH, Lang, Austria. X-rays diffraction (XRD) measurements have been performed using Cu Kα radiation with a Siemens D-500 X-ray diffractometer (Malvern Panalytical, Malvern WR14 1XZ UK).

2.2. Characterization methods

Microstructural studies were carried out using electron microscopy techniques. The scanning electron microscope (SEM) FEI E-SEM XL30 (manufactured by FEI, Hillsborough, OR, USA) was used for prior inspection of microstructure. It was equipped with EDAX Genesis EDS spectrometer (FEI, Hillsborough, OR, USA). In order to obtain the composition contrast between different phases in the sample, the backscattered electron signal (BSE mode) has been chosen for the SEM images. For the study of fracture surface fractography the secondary electron signal (SE mode) was used. The microstructural studies of the HPT-deformed samples were curry out at the distance of half the radius of HPT-disks. The transmission electron microscopy (TEM) have been performed with a TECNAI G2 FEG super TWIN (200 kV) instrument (manufactured by FEI, Hillsborough, OR, USA) equipped with an energy dispersive X-ray (EDS) spectrometer produced by EDAX (AMETEK, Inc., Berwyn, PA, USA). For the production of TEM thin foils, the twin-jet polishing was performed using a D2 electrolyte in a Struers machine (Cleveland, OH, USA). The focused ion beam (FIB) technique with FIB Quanta 3 D, TECNAI FEG microscopy (30 kV) (FEI, Hillsborough, OR, USA) was used for the TEM thin foils in the case of the material subjected to HPT and following heating at 250 °C. Spot diffraction was analyzed with the TIA software for the Tecnai microscope. Phase identification was made with CARINEV3 software.

The crystal structure and phase composition of the examined alloys were studied with high-energy X-ray diffraction measurements using the beamline P07B (87.1 keV, λ = 0.0142342 nm) at DESY in Germany, Hamburg. Diffraction patterns for the phase analysis were registered in the so-called continuous mode using the area Mar345 Image Plate detector. The experimental setup for phase analyses included rotation by 180° about the ω-axis to avoid the effect of crystallographic texture. This enables much more accurate results in terms of volume fraction calculation. The obtained 2D data were converted by the Fit2D software and presented in a graph of relative intensity versus the 2 Theta angle. Rietveld refinement and volume fraction calculations were performed using HighScore Plus software.

The *in situ* XRD measurements were carried out using CuKα radiation by the Panalytical Empyrean equipment (manufactured by the Malvern Panalytical, Malvern WR14 1XZ UK). It included the Anton Paar HTK 1200 chamber for high temperature measurements. The bulk samples were placed on an Al_2O_3 sample holder and introduced into the chamber, which was subsequently evacuated, then flushed and filled with high purity (6 N) Ar gas. Samples were heated at a rate of 5°C/min, and diffraction patterns were collected in the 40–940°C temperature range with a step size of 20°C. The 2θ range was chosen between 30 and 80° with a step size of 0.033°. The acquisition time per single pattern was 25 min preceded by 10 min of temperature stabilization.

2.3. Mechanical properties measurement methods

The AGILENT G200 nanoindenter (produced by Keysight Technologies, Santa Rosa, CA, USA) with XP head has been used for the hardness measurements at a load of 96 mN. The hardness was measured along the radius of the HPT deformed discs with the step of 50 μm starting in the centre and finishing at the edge of the sample. Each hardness value is an average of 10 measurements. Tensile test was carried out by the Instron 5566 apparatus operating at a strain rate of $10^{-3}s^{-1}$ at ambient temperature. Four flat miniature tensile specimens (with sizes about 10x1x0.2 mm) were cut from the middle of two HPT-disks using electrospark machine. Two such tensile specimens before tension were preliminarily heated in the XRD *in-situ* chamber at 250 °C for 10 min in order to partially dissolve the ω-phase. The results of tensile tests were plotted in the "engineering stress"– "engineering strain" coordinates.

3. Results and discussion

The measurements of chemical composition by the EDS/SEM method showed that the as-cast Ti–3wt.% Nb alloy contains 96.8 ± 1.9 wt%Ti and 3.2 ± 0.5 wt%Nb. The SEM observations of microstructure after annealing at 600 °C showed the presence of a small amount of β-phase precipitates, uniformly distributed in the α-matrix (Fig. 1a). Since the β-phase grains are enriched in niobium, they appear to be bright in contrast to the dark α-matrix in the micrographs taken in BSE mode (Fig. 1a). Using precise phase separation on SEM images, the volume fraction of the β-phase was evaluated as ~8%. In Fig. 1b the TEM micrograph is shown together with selected area electron diffraction patterns (SAED). It permitted to identify the second phase precipitates as a β-phase surrounded by the α-matrix. Measurements of the chemical composition by means of EDS using TEM showed about 3.0 and 14 wt% Nb in the α-matrix and the β-phase, respectively.

Fig. 2 shows the XRD curves measured using synchrotron radiation for the Ti–3wt.% Nb alloy before HPT (bottom curve) and after HPT (top curve). XRD analysis showed that both α- and β-phases are present in the initial state. The volume fraction of the α-phase reaches about 90%. After HPT the XRD peaks are much broader in comparison with the initial state, which is typical due to strong grain refinement. The intensity of the α-phase peaks strongly decreased and a lot of peaks from the ω-phase appeared, the volume fraction of which is about 80%. The main peak (00.2) of the α-phase completely disappeared after HPT, since the α→ω phase transformation takes place under the shear strain along the (00.1) planes [35]. It should be noted that two β-phase peaks (observed in the initial state) overlap with the ω-phase peaks formed after HPT. Hence it is difficult to calculate the amount of the β-phase remaining after HPT. However, in Ti-based alloys the ω-phase is more easily formed from the β-phase, especially under the action of shear stress, due to the large dimensional and structural similarities between these phases. For example, recently it was found that even a 0.1 rotation of HPT plungers for the Ti–4wt.%Fe alloy in the β-state led to the formation of 90% of the ω-phase [24]. Therefore, it is possible that the β-phase (the volume fraction of which was about 8–10% in the initial state) completely transformed into the ω-phase during HPT, while the α-Ti phase almost fully transformed into the ω-Ti phase.

Sinha et al. in their work [36] that HPT of cold rolled pure Ti resulted in the formation of ω-phase, which volume fraction, distribution and grain size depended on the texture of initial samples. For example, the ω-phase transformation was initiated first in the prismatic-pyramidal textured sample, and the basal textured sample showed a higher ω-volume fraction at higher strain. Since the ω-phase affects the hardness of the alloy, this paper also shows the relationship between the initial texture and microhardness of HPT-samples. Therefore, the study of texture is very important for study of phase transformations and mechanical properties. However, the influence of texture on the formation of the ω-phase was not taken into account in the current work because the initial state of the Ti–3wt.% Nb alloy after annealing did not show any preferential orientation indicating random texture according to the EBSD study.

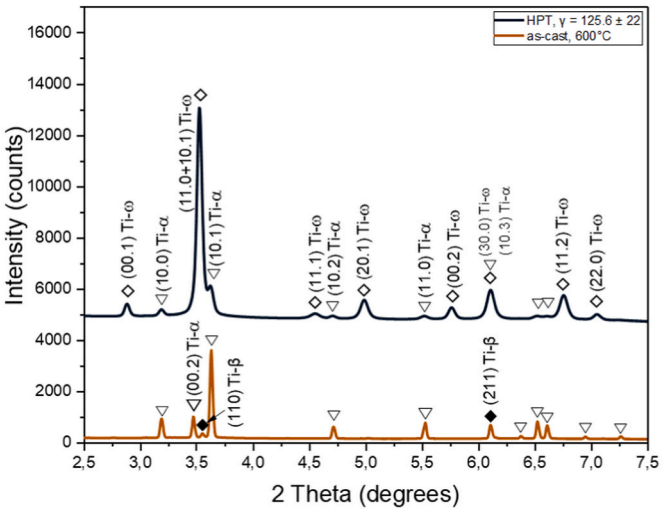

Fig. 2. (a) Synchrotron XRD curves of the Ti–3wt.% Nb alloy before (lower curve) and after (upper curve) HPT, pre-annealed at 600 °C.

The results of TEM microstructure observations of the samples after HPT are presented in Fig. 3. These are the bright field (BF) and dark field (DF) images, as well as SAED patterns (with a large number of rings). They demonstrate that the grain size during HPT strongly decreased to size of about 100 nm (Fig. 3a–c). The SAED pattern (Fig. 3c) contains no reflections from the β-phase, many reflexes (rings) of the ω-Ti phase, and just one ring of the α-Ti phase. It should be noted that in the case of XRD analysis, the broadening of the peaks and their overlapping after HPT do not allow for accurate phase separation. On the other hand, for the SAED pattern obtained by TEM, the reflections lying on the rings enable precise determination of interplanar distances and identification of the phases. Moreover, in the previous work [31], high-resolution TEM studies of this state were additionally carried out, which confirmed the presence of the α- and ω-phases, only. Therefore, it can be concluded, that under the action of HPT treatment the β-Ti phase completely transforms into ω-Ti phase, and α-Ti phase partially transforms into ω-Ti one. TEM observations of microstructure at high magnification show the presence of small grains of rounded shape and large grains of irregular shape with distinctive streaky contrast (Fig. 3d–g). The morphology of the large grains is similar to the HPT-induced ω-phase [30], while the small grains belong to the α-phase. This was confirmed by analysis of the selected area electron diffraction, presented in Fig. 3e. Ring 1 in the SAED pattern in Fig. 3e shows mainly reflexes (10.1) of the ω-phase, and corresponds to the dark field in Fig. 3f, where large grains of irregular shape with distinctive streaky contrast are clearly visible. Ring 2 in Fig. 3e contains individual reflexes, the interatomic distance of which

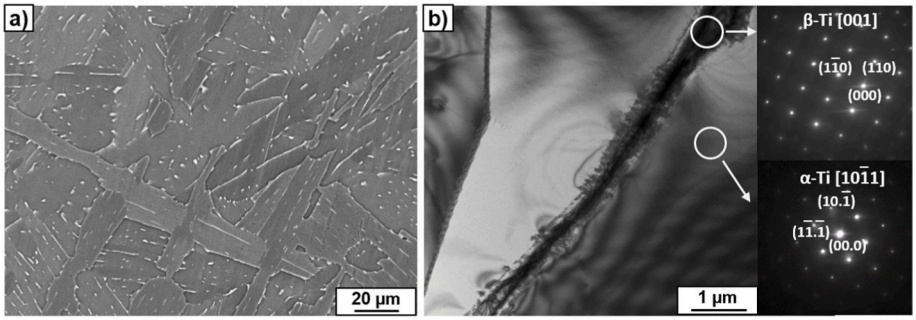

Fig. 1. (a) SEM and (b) TEM micrographs of the Ti–3wt.% Nb alloy annealed at 600 °C. Bright field image (b) with SAED patterns indicated the β- and α-phases. The white circles marked in the image (b) show the areas from which SAED patterns were obtained.

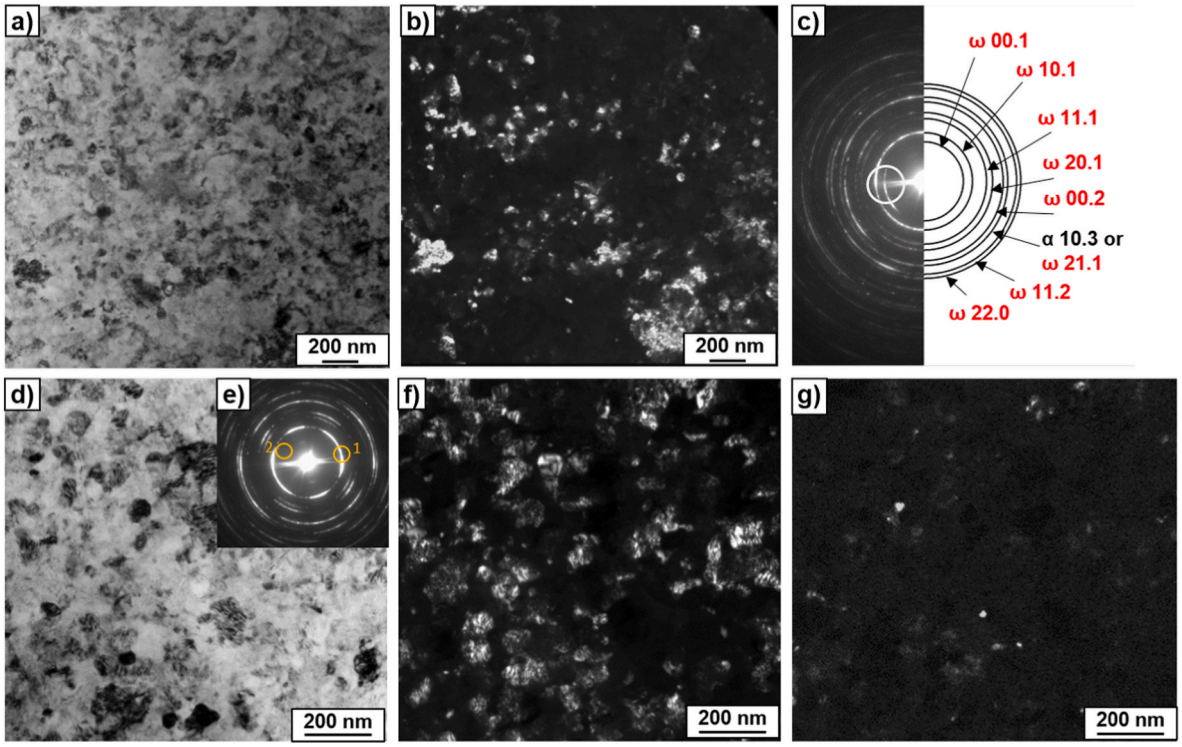

Fig. 3. (a) SEM and (b–g) TEM micrographs of the Ti–3wt.% Nb alloy after annealing and HPT process. Bright field (a, d), dark field (b, f, g) images, as well as the SAED pattern (c, g). The rings in SAED patterns indicate the position of the objective aperture for obtaining the dark-field images. Rings 1 and 2 in (e) correspond to (f) and (g) dark field images, respectively.

corresponds to the reflexes (10.0) of the α-phase. Ring 2 is responsible for the dark field in Fig. 3g, where a few small grains of rounded shape are visible.

The thermal stability of the HPT-induced ω-phase was studied by means of *in situ* XRD investigations and differential scanning calorimetry (DSC) [31]. Fig. 4a presents an *in situ* XRD pattern in the range of 2θ angles between 33 and 42° for the sample after HPT-deformation. Before heating of the deformed sample, only the (11.0)+(10.1) peak of the ω-phase can be observed clearly. Heating up to 200 °C led to a significant decrease in the intensity of the ω-phase peak and the appearance of the (10.0), (00.2) and (10.1) α-phase peaks. After heating up to 250 °C, the ω-phase fully disappeared (Fig. 4a). Therefore, it can be concluded, that the reverse transformation of ω-Ti phase to α-Ti phase proceeds between 200 and 250 °C. K. Edalati et al. [37] suggested that energy barrier for the reverse ω→α transformation is controlled by the lattice self-diffusion. Most probably, the α-phase, which formed from the disappeared ω-phase, was Nb-enriched because the ω-phase was also enriched in Nb similar to the Fe-rich ω-phase in Ti–Fe alloys [18,25]. At heating temperatures above 600 °C, the peaks of α-Ti phase slightly shifted towards the lower 2θ angles. It occurs because during the heating the new portions of α-Ti phase form, which contain less niobium. Additionally, the shift of α-Ti peaks can be driven by the thermal expansion. The similar behavior of α-Ti peaks has been observed by heating of the HPT-deformed Ti–4wt.% Co alloy [29].

Before tensile tests, four flat 1 mm thick tensile samples were cut from the central part of two HPT-deformed samples. Two specimens were used in the tensile test and marked as HPT-deformed samples. Another two specimens were preheated in the X-ray *in-situ* chamber up to a temperature of 250 °C for 10 min under a protective Ar (6 N) atmosphere. It was done in order to partially dissolve the ω-phase. Then, the X-ray *in-situ* chamber was slowly cooled at 5 °C/min together with samples in order to avoid introducing internal stresses from cooling into the specimens. Example of XRD patterns of these specimens before and after heating at 250 °C are shown in Fig. 4b. These XRD patterns indicate

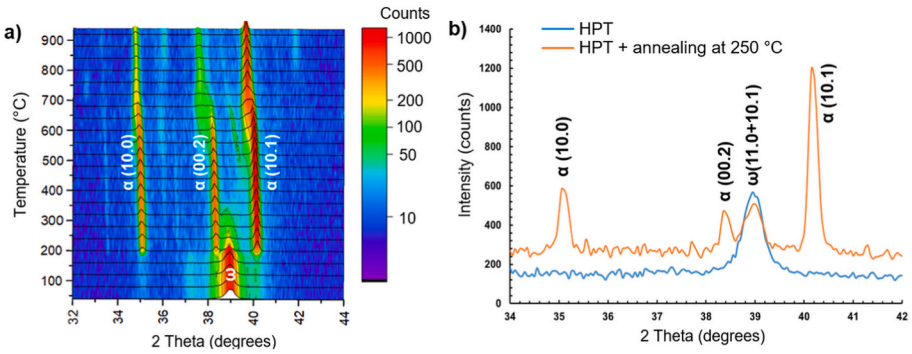

Fig. 4. (a) The XRD *in situ* heating map of the Ti–3wt.% Nb alloy after HPT. At the given 2θ angle interval, the ω-phase is presented by (11.0 + 10.1) doublet of peaks. (b) The part of the XRD patterns of the examined alloy after HPT (blue curve) and after HPT and heating at 250 °C (brown curve). (For interpretation of the references to colour in this figure legend, the reader is referred to the Web version of this article.)

that after heating the volume fraction of the ω-Ti phase decreased from 80% to only 10%.

The microstructure of a thin foil of the specimen after HPT and heating at 250 °C is shown in Fig. 5. This thin foil was cut from the deformed and heated sample by means of the focused ion beam technique. Thus, the plane of this foil was perpendicular to the foil thinned by the conventional twin-jet polishing method, the images of which are shown in Fig. 3. The investigated foil is characterised by the presence of elongated crystallites with a transverse size from 200 to 600 nm (Fig. 5a). Some of the observed crystallites still possess a high density of dislocations (even after heating), while others seem to be free of them. The SAED pattern obtained from the area visible in the BF image presented in Fig. 5a contains reflections lying along the rings. Most of them can be attributed to the α-Ti phase and a few correspond to the ω-Ti phase (Fig. 5b). Thus, after the heat-treatment at 250 °C of the sample after HPT the grain size slightly increased, the dislocation density decreased, and the ω-phase almost completely was decomposed. Fig. 5c and d, present the BF and DF images obtained at higher magnification. The DF image shows large sections of a single-phase region, surrounded by many small grains. The SAED pattern obtained from Fig. 5c contains two types of diffraction (the point and the circular) in one picture (Fig. 5e and f). Fig. 5e shows the solution for point diffraction, and Fig. 5f for circular diffraction. The point diffraction corresponds to a large α-grain with the zone axis [3-1-2-1] (Fig. 5e), while the ring diffraction belongs equally to the small crystallites of the ω-Ti and α-Ti phases. Since the DF image was taken from two rings of the ω-phase (indicated by a bright circle in Fig. 5f), the bright grains in the DF correspond to the ω-phase. Therefore, one big grain of the α-phase, inside which there are a lot of small grains of the α- and ω-phases, is observed in Fig. 5c and d. It is possible that small α-grains are formed during the reverse ω-Ti to α-Ti phase transition.

Fig. 6a shows the stress-strain dependences for the Ti–3wt.% Nb alloy obtained in the tensile test at 25°C. In these curves, the transition from elastic to plastic stage deformation occurs smoothly, without any jump. The inclination angle of tensile curves in the stage of elastic deformation permits to calculate the Young's modulus. It can be seen that the inclination angle of the curve in the initial state (black curve) coincides with the angle of the state after deformation with subsequent heating (blue curve). In these states, the samples are characterized by the presence of 90% of the α-phase in the structure. In the deformed state, the main structural component is the ω-Ti phase, the Young's modulus of which is about 130 GPa [26]. The Young's modulus of the ω-Ti phase is higher than that of α-Ti (100 GPa) [38]. Therefore the inclination angle of the curve of the deformed state (red) is greater than that of the curves corresponding to the α-phase state. The average ultimate strength values reached 289.9 ± 13.6, 625.3 ± 8.3 and 582.8 ± 4.1 MPa, respectively, for the initial state, after HPT and after HPT with subsequent heating. It should be noted that only the deformed sample destructed during tension, its plasticity being about 24%. The drop in force on other curves is associated with slippage of thin, flat samples from the handles of the tensile machine. It is difficult to find literature data on the tension of Ti–Nb alloys, so it is not possible to compare the obtained data with the literature. However, the tension of commercially pure titanium (grade 2) in the α-phase state showed that the ultimate strength reached about 250–300 MPa (depending on the tension rate), while the ductility was about 65% [22]. The HPT of this state at room temperature (five revolutions, 6 GPa) also resulted in a partial transformation of α-Ti into ω-Ti phase. The tension of the HPT-treated sample at a temperature of 200 °C (which may be similar to preheating) led to the increase of its ultimate strength up to 470–640 MPa and to the increase of plasticity up to 80–100% [22]. It has been observed earlier that HPT of the Zr-2.5 wt%Nb alloy with similar phase composition (95% α-Zr + 5% β-Zr) also led to the α → ω phase transition, and the volume fraction of the ω-Zr after HPT was about 85% [34]. Annealing between 250 and 350 °C led to the reverse ω-Zr→α-Zr transition and to a decrease in the volume fraction of ω-Zr phase to 5%. With increasing annealing temperature, the tensile strength decreased ductility increased comparing to the state after HPT. Similarly, an increase in ductility and a slight decrease in strength of the Ti–3 wt % Nb alloy was also observed in this work after HPT and subsequent heating. It should be noted that the strength data obtained in this work correlate well with the microhardness data of the examined alloy (Fig. 6b). Here, the microhardness of the initial state reached 2.7 ± 0.4 GPa, after HPT: 5.8 ± 0.2, and after HPT with subsequent heating was 4.4 ± 0.4 GPa. The decrease in hardness after heating of the deformed state is associated with the decrease of the ω-Ti volume fraction, with slight grain growth, and with a decrease in the density of crystalline defects appeared after HPT.

The micro-fractography of the HPT-deformed sample after the tensile test is presented in Fig. 7. The fracture surface is highly developed (Fig. 7a), i.e. it is not flat and perpendicular to the tension axis. This type

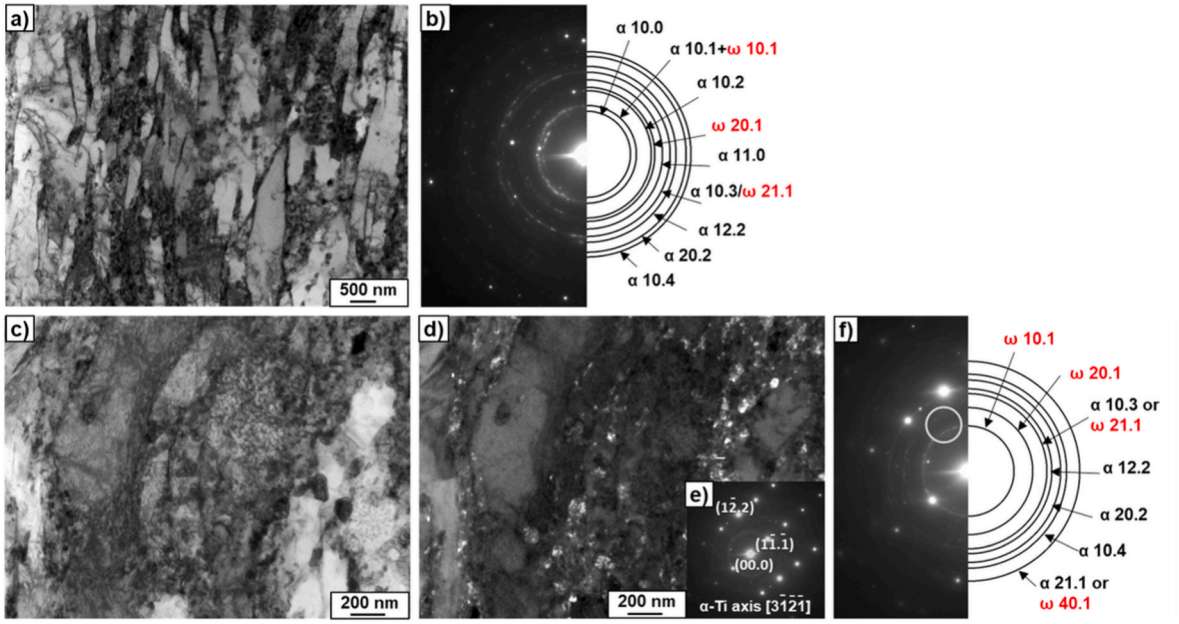

Fig. 5. TEM micrographs of the Ti–3wt.% Nb alloy after HPT and heating at 250 °C. Bright field images (a, c), dark field image (d) and SAED patterns (b, e, f).

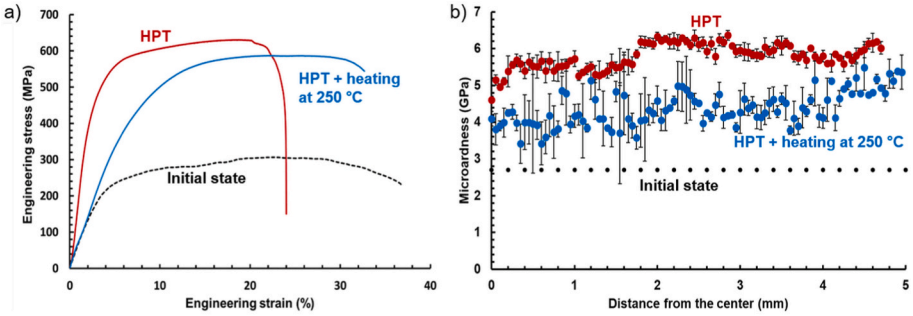

Fig. 6. (a) Stress-strain curves of the Ti–3wt.% Nb alloy in the different states. (b) Values of the microhardness across radius of the sample subjected HPT and HPT followed by heating at 250 °C. The dotted line show the hardness in the initial state.

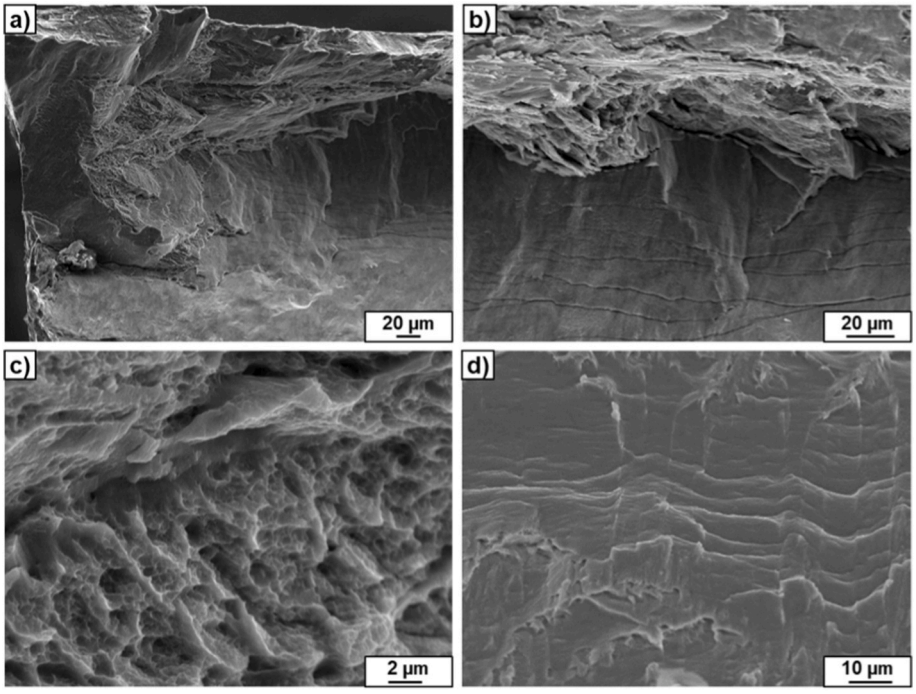

Fig. 7. The fractography of the HPT-deformed sample subjected to tension.

of fracture is characteristic to the plastic fracture [39]. The plastic fracture takes place above the yield point and requires a continuous supply of external energy. Plastic deformation is caused by slip (shear) in the slip planes (Fig. 7a and b) and at the grain boundaries (Fig. 7c). One can also see the elements of a transcrystalline splintery (brittle) fracture with a flat fracture surface (Fig. 7b) and in the form of characteristic faults (Fig. 7d). Therefore, it can be concluded that the observed fracture of the HPD-deformed sample has a character of mixed ductile-brittle fracture.

4. Conclusions

HPT of the Ti–3wt.% Nb alloy led to the strong grain refinement, partial α-Ti → ω-Ti as well as complete β-Ti → ω-Ti phase transformations. The reverse ω-Ti → α-Ti transformation proceed between 200 and 250°C. The measurement of mechanical properties by tensile testing showed that HPT leads to an almost two-fold increase in ultimate strength (from 300 to 630 MPa), and to a decrease in plasticity compared to the initial state. Short-term heating of the deformed state at 250 °C for 10 min led to: 1) insignificant grain growth of microstructure, 2) decomposition of the ω-phase with the preservation of its amount up to 10%, and 3) decreased density of the crystal structure defects. Such microstructural changes led to a decrease in hardness and as well as to an important increase in plasticity and a slight decrease in the ultimate strength of the alloy. The use of the HPT process followed by additional annealing seems to be very promising method for obtaining metallic biomaterials with high level of mechanical properties.

CRediT authorship contribution statement

A. Korneva: Conceptualization, Visualization, Supervision, Data curation, Investigation, Writing – original draft, Writing – review & editing, Funding acquisition. **B. Straumal:** Conceptualization, Writing – review & editing. **A. Kilmametov:** Investigation. **S. Kopacz:** Methodology, Investigation. **M. Szczerba:** Methodology, Writing – review & editing. **Ł. Gondek:** Investigation. **G. Cios:** Investigation. **L. Lityńska-Dobrzyńska:** Investigation. **R. Chulist:** Investigation.

Declaration of competing interest

The authors declare that they have no known competing financial interests or personal relationships that could have appeared to influence the work reported in this paper.

Data availability

Data will be made available on request.

Acknowledgements

This work is supported by National Science Centre of Poland (grant OPUS 2017/27/B/ST8/0 1092). SEM and TEM investigations were performed within the Accredited Testing Laboratories possessing the certificate No. AB 120 issued by the Polish Centre of Accreditation according to European standard PN-ISO/IEC 17025:2005 and the EA-2/15.

References

[1] J. Jakubowicz, Special issue: Ti-based biomaterials: synthesis, properties and applications, Materials 13 (2020) 1696, https://doi.org/10.3390/ma13071696.
[2] M. Niinomi, Design and development of metallic biomaterials with biological and mechanical biocompatibility, J. Biomed. Mater. Res. 107 (2019) 944–954, https://doi.org/10.1002/jbm.a.36667.
[3] A. Campos-Quirós, J.M. Cubero-Sesín, K. Edalati, Synthesis of nanostructured biomaterials by high-pressure torsion: effect of niobium content on microstructure and mechanical properties of Ti-Nb alloys, Mater. Sci. Eng., A 795 (2020) 139972, https://doi.org/10.1016/j.msea.2020.139972.
[4] M. Bönisch, M. Calin, T. Waitz, A. Panigrahi, M. Zehetbauer, A. Gebert, W. Skrotzki, J. Eckert, Thermal stability and phase transformations of martensitic Ti–Nb alloys, Sci. Technol. Adv. Mater. 14 (2013), 055004. https://www.tandfonline.com/doi/pdf/10.1088/1468-6996/14/5/055004.
[5] M.A. Khimich, K.A. Prosolov, T. Mishurova, S. Evsevleev, X. Monforte, A. H. Teuschl, P. Slezak, E.A. Ibragimov, A.A. Saprykin, ZhG. Kovalevskaya, A. I. Dmitriev, G. Bruno, YuP. Sharkeev, Advances in laser additive manufacturing of Ti-Nb alloys: from nanostructured powders to bulk objects, Nanomaterials 11 (2021) 1159, https://doi.org/10.3390/nano11051159.
[6] R.Z. Valiev, Y. Estrin, Z. Horita, T.G. Langdon, M.J. Zehetbauer, Y.T. Zhu, Producing bulk ultrafine-grained materials by severe plastic deformation, J. Occup. Med. 58 (4) (2006) 33–39. https://link.springer.com/content/pdf/10.1007/s11837-006-0213-7.pdf.
[7] V. Segal, Review: modes and processes of severe plastic deformation (SPD), Materials 11 (2018) 1175, https://doi.org/10.3390/ma11071175.
[8] K. Edalati, A. Bachmaier, V.A. Beloshenko, Ya Beygelzimer, V.D. Blank, W.J. Botta, K. Bryła, Ja Čížek, S. Divinski, N.A. Enikeev, Yu Estrin, G. Faraji, R.B. Figueiredo, M. Fuji, T. Furuta, T. Grosdidier, Je Gubicza, A. Hohenwarter, Ze Horita, Ja Huot, Yo Ikoma, M. Janeček, M. Kawasaki, P. Král, Sh Kuramoto, T.G. Langdon, D. R. Leiva, V.I. Levitas, A. Mazilkin, M. Mito, H. Miyamoto, T. Nishizaki, R. Pippan, V.V. Popov, E.N. Popova, G. Purcek, O. Renk, Á. Révész, X. Sauvage, V. Sklenika, W. Skrotzki, B.B. Straumal, S. Suwas, L.S. Toth, N. Tsuji, R.Z. Valiev, G. Wilde, M. J. Zehetbauer, X. Zhu, Nanomaterials by severe plastic deformation: review of historical developments and recent advances, Mater. Res. Lett. 4 (2022) 163–256, https://doi.org/10.1080/21663831.2022.2029779.
[9] J. Gubicza, Zs Fogarassy, Gy Krállics, J. Lábár, T. Törköly, Microstructure and mechanical behavior of ultrafine-grained titanium, Mater. Sci. Forum 589 (2008) 99–104. https://doi.org/10.4028/www.scientific.net/MSF.589.99.
[10] R.K. Islamgaliev, V.U. Kazyhanov, L.O. Shestakova, A.V. Sharafutdinov, R. Z. Valiev, Microstructure and mechanical properties of titanium (Grade 4) processed by high-pressure torsion, Mater. Sci. Eng. 493 (2008) 190–194, https://doi.org/10.1016/j.msea.2007.08.084.
[11] T. Lee, Y.U. Heo, C.S. Lee, Microstructure tailoring to enhance strength and ductility in Ti–13Nb–13Zr for biomedical applications, Scripta Mater. 69 (2013) 785–788, https://doi.org/10.1016/j.scriptamat.2013.08.028.
[12] H. Matsumoto, S. Watanabe, Sh Hanada, Beta TiNbSn alloys with low young's modulus and high strength, Mater. Trans. 46 (5) (2005) 1070–1078, https://doi.org/10.2320/matertrans.46.1070.
[13] O. Kashin, K. Krukovskii, A. Lotkov, V. Grishkov, Effect of true strains in isothermal *abc* pressing on mechanical properties of Ti49.8Ni50.2 alloy, Metals 10 (2020) 1313, https://doi.org/10.3390/met10101313.
[14] N.N. Kuranova, V.V. Makarov, V.G. Pushin, A.N. Uksusnikov, Thermo- and deformation induced martensitic transformations in binary tini-based alloys subjected to severe plastic deformation, Mater. Sci. Forum 738–739 (2013) 530–534. https://doi.org/10.4028/www.scientific.net/MSF.738-739.530.
[15] Y. Zhentao, M. Xiqun, W. Gui, Y. Sen, S. Qiaoyan, D. Kent, Microstructure and mechanical properties of biomedical near-p ti alloy TLM with nanostructure by ARB process, 12th World Conference on Titanium (Ti-2011), in: Proceedings of the 12th World Conference on Titanium 3, 2012, pp. 2054–2058.
[16] D.L. Moffat, U.R. Kattner, The stable and metastable Ti-Nb phase diagrams, Metall. Trans. A 19 (1988) 2389–2398. https://link.springer.com/content/pdf/10.1007/BF02645466.pdf.
[17] J. Xu, W. Zeng, Ya Zhao, X. Sun, Z. Du, Influence of cooling rate following heat treatment on microstructure and phase transformation for a two-phase alloy, J. Alloys Compd. 688 (2016) 301–309, https://doi.org/10.1016/j.jallcom.2016.07.107.
[18] Yu Ivanisenko, A. Kilmametov, H. Rösner, R.Z. Valiev, Evidence of α → ω phase transition in titanium after high pressure torsion, Int. J. Mater. Res. 90 (2008) 36–41, https://doi.org/10.3139/146.101606.
[19] D. Errandonea, Y. Meng, M. Somayazulu, D. Häusermann, Pressure-induced α→ω transition in titanium metal: a systematic study of the effects of uniaxial stress, Physica B 355 (2005) 116–125, https://doi.org/10.1016/j.physb.2004.10.030.
[20] A.K. Singh, M. Mohan, C. Divakar, Pressure-induced alpha-omega transformation in titanium: features of the kinetics data, J. Appl. Phys. 54 (1983) 5721–5730, https://doi.org/10.1063/1.331793.
[21] A.P. Zhilyaev, S.N. Sergeev, V.A. Popov, A.V. Orlov, Evolution of microstructure and microhardness in HPT titanium during annealing, Rev. Adv. Mater. Sci. 39 (2014) 15–19. H:\Work\RAMS39~1\03_Zhilyaev.pm (nw.ru), https://www.scribd.com/document/274067980/Evolution-of-Microstructure-and-Microhardness-in-Hpt-Titanium-During-Annealing.
[22] M. Shirooyeh, J. Xu, T.G. Langdon, Microhardness evolution and mechanical characteristics of commercial purity titanium processed by high-pressure torsion, Mater. Sci. Eng. 614 (2014) 223–231, https://doi.org/10.1016/j.msea.2014.07.030.
[23] B. Straumal, A. Korneva, A. Kilmametov, L. Lityńska-Dobrzyńska, A. Gornakova, R. Chulist, M. Karpov, P. Zięba, Structural and mechanical properties of Ti–Co alloys treated by high pressure torsion, Materials 12 (2019) 426, https://doi.org/10.3390/ma12030426.
[24] A.R. Kilmametov, Yu Ivanisenko, A.A. Mazilkin, B.B. Straumal, A.S. Gornakova, O. B. Fabrichnaya, M.J. Kriegel, D. Rafaja, H. Hahn, The α→ω and β→ω phase transformations in Ti-Fe alloys under high-pressure torsion, Acta Mater. 144 (2018) 337–351, https://doi.org/10.1016/j.actamat.2017.10.051.
[25] A. Kilmametov, Yu Ivanisenko, B. Straumal, A.A. Mazilkin, A.S. Gornakova, M. J. Kriegel, O.B. Fabrichnaya, D. Rafaja, H. Hahn, Transformations of α' martensite in Ti–Fe alloys under high pressure torsion, Scripta Mater. 136 (2017) 46–49, https://doi.org/10.1016/j.scriptamat.2017.04.010.
[26] A. Panigrahi, M. Bönisch, T. Waitz, E. Schafler, M. Calin, J. Eckert, W. Skrotzki, M. Zehetbauer, Phase transformations and mechanical properties of biocompatible Ti–16.1Nb processed by severe plastic deformation, J. Alloys Compd. 628 (2015) 434–441, https://doi.org/10.1016/j.jallcom.2014.12.159.
[27] N. Adachi, Y. Todaka, K. Irie, M. Umemoto, Phase transformation kinetics of x-phase in pure Ti formed by high-pressure torsion, J. Mater. Sci. 51 (2016) 2608–2615, https://doi.org/10.1007/s10853-015-9574-z.
[28] M.J. Kriegel, A. Kilmametov, M. Rudolph, B.B. Straumal, A.S. Gornakova, H. Stöcker, Y. Ivanisenko, O. Fabrichnaya, H. Hahn, D. Rafaja, Transformation pathway upon heating of Ti–Fe alloys deformed by high-pressure torsion, Adv. Eng. Mater. 20 (2018), 1700933, https://doi.org/10.1002/adem.201700933.
[29] A. Korneva, B.B. Straumal, A.R. Kilmametov, Ł. Gondek, A. Wierzbicka-Miernik, L. Lityńska-Dobrzyńska, R. Chulist, G. Cios, P. Zięba, The α↔ω phase transformations and thermal stability of Ti-Co alloy treated by high pressure torsion, Mater. Char. 173 (2021), 110937, https://doi.org/10.1016/j.matchar.2021.110937.
[30] A. Shurygina, A.O. Cheretaeva, A.M. Glezer, D.L. D'yakonov, I.V. Chshetinin, R. V. Sundeev, A.A. Tomchuk, L.F. Muradimova, Effect of the temperature of megaplastic deformation in a bridgman chamber on the formation of structures and the physicochemical properties of titanium (BT1-0), B. Russ, Acad. Sci.: Physics 82 (9) (2018) 1113–1124, https://doi.org/10.3103/S1062873818090204.
[31] A. Korneva, B. Straumal, A. Kilmametov, A. Gornakova, A. Wierzbicka-Miernik, L. Lityńska-Dobrzyńska, R. Chulist, Ł. Gondek, G. Cios, P. Zięba, Omega phase formation in Ti–3wt.%Nb alloy induced by high-pressure torsion, Materials 14 (2021) 2262, https://doi.org/10.3390/ma14092262.
[32] R.Z. Valiev, A.V. Sergueeva, A.K. Mukherjee, The effect of annealing on tensile deformation behawior of nanostructured SPD titanium, Scripta Mater. 49 (2003) 669–674, https://doi.org/10.1016/S1359-6462(03)00395-6.
[33] A.V. Sergueeva, V.V. Stolyarov, R.Z. Valiev, A.K. Mukherjee, Advanced mechanical properties of pure titanium with ultrafine grained structure, Scripta Mater. 45 (2001) 747–752, https://doi.org/10.1016/S1359-6462(01)01089-2.
[34] S.O. Rogachev, S.A. Nikulin, V.M. Khatkevich, M.V. Gorshenkov, R.V. Sundeev, A. A. Veligzhanin, Effect of annealing on structural and phase transformations and mechanical properties of ultrafine-grained E125 zirconium alloy obtained by high-pressure torsion, Mater. Lett. 206 (2017) 26–29, https://doi.org/10.1016/j.matlet.2017.06.107.
[35] D.R. Trinkle, R.G. Hennig, S.G. Srinivasan, D.M. Hatch, M.D. Jones, H.T. Stokes, R. C. Albers, J.W. Wilkins, New mechanism for the α to ω martensitic transformation in pure titanium, Phys. Rev. Lett. 91 (2003), 025701.
[36] S. Sinha, V.K. Sahu, V. Beura, R. Sonkusare, R. Kalsar, A.K.L. Das, J. Basu, N. P. Gurao, K. Biswas, Initial texture dependence of nanocrystalline omega phase formation during high pressure torsion of commercially pure titanium, Mater. Sci. Eng. 802 (2021) 140687, https://doi.org/10.1016/j.msea.2020.140687.
[37] K. Edalati, T. Daio, M. Arita, S. Lee, Z. Horita, A. Togo, I. Tanaka, High-pressure torsion of titanium at cryogenic and room temperatures: grain size effect on allotropic phase transformations, Acta Mater. 68 (2014) 207–213, https://doi.org/10.1016/j.actamat.2014.01.037.
[38] Y. Fua, W. Xiao, J. Wang, L. Ren, X. Zhao, C. Ma, A novel strategy for developing α + β dual-phase titanium alloys with low Young's modulus and high yield strength, J. Mater. Sci. Technol. 76 (2021) 122–128, https://doi.org/10.1016/j.jmst.2020.11.018.
[39] W. Dziadur, J. Mikuła, Mikroskopia Elektronowa, , Tom III Praktyczna Mikroskopia skaningowa, Politechnika Krakowska im T. Kościuszki, Kraków (2019) 329–335 (in Polish).